Atomic Resolution Crystal Structures, EXAFS, and Quantum Chemical Studies of Rusticyanin and Its Two Mutants Provide Insight into Its Unusual Properties[†,‡]

Mark L. Barrett,[§,||] Ian Harvey,[||] Mahesh Sundararajan,[⊥] Rajeev Surendran,[⊥] John F. Hall,[§,||] Mark J. Ellis,[||] Michael A. Hough,[||] Richard W. Strange,[||] Ian H. Hillier,*[,⊥] and S. Samar Hasnain*[,§,||]

School of Health and Life Sciences, De Montfort University, The Gateway, Leicester LE1 9BH, U.K., CCLRC Daresbury Laboratory, Warrington, Cheshire WA4 4AD, U.K., and School of Chemistry, University of Manchester, Oxford Road, Manchester M13 9PL, U.K.

Received November 21, 2005; Revised Manuscript Received December 22, 2005

ABSTRACT: Rusticyanin from the extremophile *Thiobacillus ferrooxidans* is a blue copper protein with unusually high redox potential and acid stability. We present the crystal structures of native rusticyanin and of its Cu site mutant His143Met at 1.27 and 1.10 Å, respectively. The very high resolution of these structures allows a direct comparison with EXAFS data and with quantum chemical models of the oxidized and reduced forms of the proteins, based upon both isolated and embedded clusters and density functional theory (DFT) methods. We further predict the structure of the Cu(II) form of the His143Met mutant which has been experimentally inaccessible due to its very high redox potential. We also present metrical EXAFS data and quantum chemical calculations for the oxidized and reduced states of the Met148Gln mutant, this protein having the lowest redox potential of all currently characterized mutants of rusticyanin. These data offer new insights into the structural factors which affect the redox potential in this important class of proteins. Calculations successfully predict the structure and the order of redox potentials for the three proteins. The calculated redox potential of H143M (∼400 mV greater than native rusticyanin) is consistent with the failure of readily available chemical oxidants to restore a Cu(II) species of this mutant. The structural and energetic effects of mutating the equatorial cysteine to serine, yet to be studied experimentally, are predicted to be considerable by our calculations.

Rusticyanin is a monomeric type I "blue" copper protein of 155 amino acids and is thought to be a principal component in the iron respiratory electron transport chain of the Gram-negative, acidophilic bacterium *Thiobacillus ferrooxidans* (*1*), also known as *Acidothiobacillus ferrooxidans* (*2*). The protein is tolerant of an extremely wide pH range (1.5−9.0) and exhibits optimal redox activity around pH 2 with some activity even at pH 0.5 (*3*). In addition to this remarkable property, rusticyanin has a Cu(I)−Cu(II) redox couple of ∼680 mV (*4*, *5*) whereas more typical redox potentials for the type 1 copper proteins are around 300 mV. Crystallographic and NMR[1] studies (*6*−*8*) of native rusticyanin have shown that the protein is composed of a β-sandwich core with a Cu site very similar to that of other blue copper proteins, having a distorted trigonal planar geometry with three strong ligands, His85 $N^{\delta 1}$, Cys138 S^{γ}, His143 $N^{\delta 1}$, and a relatively weaker Met148 S^{δ} ligand in an axial position. Ser86, rather than the conserved Asn found at this position in other blue copper proteins, may provide some protection for the Cu in highly acidic media (*9*−*11*). Unique to rusticyanin is a 35-residue N-terminal extension containing three additional β-strands.

Studies by Guidici-Orticoni and co-workers (*12*) have shown that rusticyanin forms a tight complex with cytochrome c_4, and the exposed histidine ligand (His143) is likely to be a key residue in the formation of the complex, consistent with observations of other blue copper proteins (*13*−*15*). The redox potential of rusticyanin in the complex was lowered by 100 mV compared to its value in free rusticyanin, leading to the suggestion that His143 acts as a "redox switch". The solvent-exposed histidine has been a subject of site-directed mutagenesis in azurin (*16*) and the type 1 Cu site of *Alcaligenes xylosoxidans* nitrite reductase

[†] This work was supported by BBSRC Grants (719/B06916 and 719/B14224) to S.S.H.

[‡] Coordinates and structure factors have been deposited in the Protein Data Bank, accession codes 2cak (native) and 2cal (H143M).

* To whom correspondence should be addressed. S.S.H.: tel, +44 (0) 1925 603273; e-mail, S.Hasnain@dl.ac.uk. I.H.H.: tel, +44 (0) 161 275 4686; fax, +44 (0) 161 275 4734; e-mail, Ian.Hillier@manchester.ac.uk.

[§] De Montfort University.

[||] CCLRC Daresbury Laboratory.

[⊥] University of Manchester.

[1] Abbreviations: ADE, adiabatic detachment energy; AMBER, assisted model building with energy refinement; AxNiR, *Alcaligenes xylosoxidans* nitrite reductase; C138S, cysteine 138 mutated by serine; DFT, density functional theory; BP86, Becke and Perdew, 1986; EE, electronic embedding; EXAFS, extended X-ray absorption fine structure; EPR, electron paramagnetic resonance; FPLC, fast-performance liquid chromatography; H143M, histidine 143 mutated by methionine; Im, imidazole; M148Q, methionine 148 mutated by glutamine; ME, mechanical embedding; MM, molecular mechanics; NMR, nuclear magnetic resonance; ONIOM, our own N-layered integrated molecular orbital and molecular mechanics; PDB, Protein Data Bank; QM, quantum mechanics; Rc, rusticyanin; RMS, root mean square; TIP3P, transferable intermolecular potential-3-point-charge water model; TZV*, triple-ζ valence polarization; VAE, vertical attachment energy; VDE, vertical detachment energy; XRF, X-ray fluorescence spectroscopy; λ, reorganization energy.

10.1021/bi052372w CCC: $33.50
Published on Web 02/07/2006

(AxNiR) (*17*). In both cases, a substantial increase in redox potential has been reported.

There have been a number of experimental and theoretical studies of the members of the family of blue copper proteins, azurin, plastocyanin, and stellacyanin (*18*−*24*). The role of different ligands coordinated to the copper center in determining the active site structure and redox properties of type 1 Cu proteins is generally understood, at least qualitatively (*25*−*27*). These proteins have in common three equatorial ligands, two histidines and one cysteine, but have different ligands in their axial positions, either methionine, glycine, or glutamine (*24*, *28*, *29*). The different electronic nature of these sulfur and oxygen binding ligands is responsible for modulating the properties of the copper center. Thus, the harder ligands (more strongly bound) Gln and Gly favor the trigonal and tetragonal structures for Cu(I) and Cu(II), respectively, while the softer methionine ligand does not favor either structure. These trends have been substantiated by theoretical studies by Ryde et al. on model compounds (*30*). The hard ligands also preferentially stabilize the higher oxidation states compared to the effect of the sulfur-containing ligands, leading to plastocyanin having the larger and stellacyanin the smaller redox potential of the three proteins, with azurin, which has both methionine and glycine in the axial positions, being intermediate (*18*, *31*).

Mutation studies have provided additional insight into the structure−function relationships of these blue copper proteins (*11*, *28*, *29*, *31*). In particular, structural studies of increasing resolution have shown that quite large geometrical changes may arise from changes in the axial ligands (*23*, *32*). However, it might be expected that mutation of the more strongly bound equatorial ligands will have a greater effect on the protein properties. In addition, to fully understand the relationship between structure and redox properties, we require accurate structural data for the protein in both oxidation states, which is often lacking. Computational studies of the geometric and electronic structures of proteins have advanced considerably over the past decade so that predictions of active site geometry and energetics can be made to an accuracy which rivals experiment (*18*, *19*, *33*). Since it is obviously not feasible to treat the whole protein at an acceptable level of quantum mechanics (QM), we use a hybrid method combining a QM description of the copper center and the ligands directly bonded to it with a molecular mechanical (MM) description of the rest of the protein. Such hybrid QM/MM models have been used quite successfully in an attempt to understand structure−function relationships in many enzymes (*34*−*36*). With the increasing availability of higher resolution protein structures, and the increasing accuracy of QM/MM calculations, there can now be much greater interaction between theory and experiment in order to probe the relationship between protein structure and function.

We here report two crystal structures of rusticyanin, the wild-type native protein at 1.27 Å resolution and a single point mutation of the solvent-accessible His143 Cu ligand, also referred to as the redox switch, His143Met (H143M) at atomic (1.10 Å) resolution. This is the first atomic resolution[2] crystal structure for rusticyanin. We also present EXAFS metrical data for H143M and also for the Cu(I) and Cu(II) states of the native rusticyanin and the Met148Gln mutant (M148Q), for which a crystal structure was recently determined (*15*). We also report new computational studies of native rusticyanin and both the axial M148Q and equatorial H143M mutants in order to gain more insight into the structure−function relationships of blue copper proteins and the determinants of redox potential. We have studied this latter mutant, since although there have been a number of studies of the effect of axial mutations on both the structure and redox potential, corresponding studies on equatorial mutants have been lacking.

EXPERIMENTAL PROCEDURES

Protein Expression and Purification. The native protein was extracted directly from *T. ferrooxidans* and purified as described previously (*4*), while the recombinant native and H143M and M148Q mutant proteins were prepared as described by Hall et al. (*28*). Prior to any crystallization, the proteins were further purified using fast-performance liquid chromatography (FPLC). Gel electrophoresis (SDS−PAGE) was performed to assess the purity of the protein fractions. Oxidation of the colorless H143M protein was attempted using K_2IrCl_6 and H_2O_2 with small aliquots of $CuSO_4$ added. No color change was observed, suggesting a redox potential in excess of 800 mV. The presence of Cu was confirmed by EXAFS.

Redox Measurements. Cyclic voltammetry was performed on an Autolab PGSTAT30 potentiostat. The electrode system consisted of an $Ag/AgCl_2$ reference, Pt counter, and Au (BAS systems) working electrode modified with Aldrithiol (4,4′-dipyridyl disulfide). The working electrode was prepared by soaking in concentrated sulfuric acid for at least 30 min followed by sonication in deionized water (5 min × 2), polishing with alumina (0.075 unit), and finally two further sonications. This gave a value of 600 mV vs SHE for native recombinant rusticyanin in phosphate buffer, 10 mM at pH 5.2, which is in good agreement with the results of Haladjian et al. (*37*) of 570 mV at pH 6.2 for the wild-type protein.

EXAFS Data Collection and Processing. The proteins were buffer exchanged into 50 mM citric acid and 100 mM MES, pH 4.0 (the same as that used in crystallization), and loaded into a EXAFS cell for freezing in liquid nitrogen. Fluorescence EXAFS data were collected on station 9.2 at the SRS, Daresbury Laboratory using methods described previously (*38*). Analysis of the data was carried out using the crystallographic coordinates with the program EXCURVE98.

Protein Crystallization. Crystals of native rusticyanin were grown in the reduced form (Cu^+) in space group $P2_1$ using conditions similar to those described previously (*39*). Plate-like colorless crystals of H143M were grown using the hanging drop vapor diffusion method at 293 K. Two microliters of 10 mg mL^{-1} protein in 10 mM H_2SO_4, pH 3.8, was mixed with an equal volume of reservoir solution consisting of 30% PEG 12K, 50 mM citric acid, and 100 mM MES, pH 4.0, and suspended over a 500 μL reservoir.

X-ray Data Collection and Processing. High-Resolution Data Collection. For native rusticyanin, data were collected at room temperature on a single crystal using a MAR 345 image plate detector on station 9.6 at the SRS, Daresbury Laboratory at a wavelength of 0.87 Å. The crystal was

[2] Atomic resolution, 1.2 Å or better, refers to that resolution where the carbon−carbon bond of the polypeptide is resolved.

Table 1: Summary of Data Collection Statistics, Final Model, and Refinement Results

	native	H143M
collection statistics		
space group	$P2_1$	$P2_1$
resolution (Å)	12−1.27	35.6−1.1
unit cell dimensions		
a (Å)	32.5	32.3
b (Å)	60.8	60.1
c (Å)	38.1	37.2
β (deg)	108.0	107.4
solvent content (%)	50.1	43.4
no. of obsd reflections	148206	824495
no. of unique reflections	37281	48379
completeness (%)[a]	99.7 (100)	89.4 (72.6)
R_{merge} (%)[a]	4.6 (39.4)	8.1 (19.9)
$I/\sigma(I)$[a]	9.7 (2.2)	11.0 (2.9)
multiplicity[a]	4.0 (3.2)	17.0 (1.7)
refinement and model quality		
R_{work}[b]	12.0	14.0
R_{free}[c]	13.5	17.0
no. of protein atoms	1197	1185
no. of water atoms	86	274
temperature factors		
Wilson (Å^2)	15.3	11.8
protein (Å^2)	18.3	16.2
Cu (Å^2)	13.4	15.0
water (Å^2)	35.2	39.7
RMS deviations		
bond distances (Å)	0.014	0.013
bond angles (deg)	1.702	1.621
Ramachandran plot		
residues in most favored regions	91.7	90.9

[a] Figures in parentheses are for the outer resolution shell, 1.30−1.27 Å (native) and 1.12−1.10 Å (H143M). [b] R_{work} calculated after inclusion of R_{free} reflections. [c] R_{free} was calculated for 4310 and 1486 reflections, respectively.

mounted in a capillary with the spindle slightly aligned along its *b*-axis so that most Friedel pairs were collected on the same image. For H143M, a single crystal was flash-cooled to 100 K in a nitrogen cryostream after being soaked for approximately 1 min in cryoprotectant solution consisting of 75% mother liquor with 25% glycerol. Data were collected on a single crystal using a Mar 165 CCD detector on station 9.5 at the SRS using an X-ray wavelength of 0.85 Å.

In both cases data were integrated using DENZO (*40*) and scaled and merged using either SCALEPACK (*40*) or the CCP4 suite (*41*). Data reduction parameters are summarized in Table 1. Both proteins crystallize in space group $P2_1$ with unit cell parameters $a = 32.5$ Å, $b = 60.8$ Å, $c = 38.1$ Å, and $\beta = 108.0°$ for native rusticyanin and $a = 32.3$ Å, $b = 60.1$ Å, $c = 37.2$ Å, and $\beta = 107.4°$ for H143M.

Structure Solution and Refinement. The two structures were solved using the molecular replacement method implemented in AMoRe (*42*) using the 2.1 Å resolution structure of native rusticyanin (PDB accession code 1A8Z) (*7*) with the waters removed as the search model. In the case of H143M residue 143 was also truncated to alanine. The solutions to the rotation and translation functions confirmed a single molecule in the asymmetric units and yielded an *R*-factor of 21.0% and 28.0% and a correlation coefficient of 88.3% and 80.3% for the native and H143M structures, respectively.

Native Rusticyanin. For native rusticyanin, refinement of the molecular replacement model was carried out initially with X-PLOR (*43*) and the Engh and Huber (*44*) parameter libraries. Simulated annealing and *B*-factor refinement resulted in an *R*-factor of 20.5%. Refinement proceeded in SHELX97 (*45*) using conjugate gradient least-squares refinement. Several cycles of refinement and model building in "O" (*46*) and the inclusion of waters reduced the *R*-factors to $R_{cryst} = 19.4\%$ and $R_{free} = 21.1\%$. Moving to restrained anisotropic refinement at this point reduced the *R*-factors by approximately 6% ($R_{cryst} = 13.3\%$, $R_{free} = 15.4\%$). The electron density map was significantly improved, allowing modeling of residue 2. The entire data set to 1.27 Å, including the 8% of reflections which were set aside for calculating R_{free} was then used for a final cycle least-squares full-matrix inversion, which yielded a final R_{cryst} of 12.0% (Table 1). The final model consists of residues 2−155, 1 Cu, and 86 waters. Analysis with PROCHECK (*47*) shows good stereochemistry with 91.7% of the residues within the Ramachandran most favored region and all other residues within the allowed region (Table 1).

H143M. Prior to any refinement, 3% (1450) of all reflections were set aside for calculation of the free *R*-factor. The model was refined using the maximum likelihood method implemented in REFMAC5 (*48*) and rebuilt using O (*46*). A total of 274 water molecules were added using ARP/wARP (*49*). No restraints were applied to the copper−ligand distances or bond angles during refinement. Stereochemical checks were performed using PROCHECK and OOPS (*50*). Several rounds of refinement and rebuilding produced a model with an *R*-factor of 16.2% ($R_{free} = 18.1\%$) using data to 1.1 Å. At this point anisotropic displacement parameters (ADP) were introduced using REFMAC5, which produced a 1.7% drop in *R*-factor (1.2% drop in R_{free}). Further refinement and the introduction of riding hydrogen atom positions then proceeded using SHELX97 (*45*) until the model converged to a final *R*-factor of 14.0% for all reflections. ($R_{free} = 17.0\%$). Refinement statistics are summarized in Table 1.

COMPUTATIONAL DETAILS

We have studied models of both the isolated active site of each protein, using density functional theory (DFT), and of the protein itself. The latter employ a hybrid QM/MM model combining a DFT description of the active site, with a MM description of the remainder of the protein. In all QM calculations we have chosen to use the hybrid functional (BP86) having 38% exchange, as suggested by Szilagyi et al. (*51*) in conjunction with TZV* and 6-31G* basis sets for copper and the remaining atoms. This combination was found to give a good description of the electronic structure of $[CuCl_4]^{2-}$. We have used two variants of the hybrid QM/MM model, depending upon whether the MM region polarizes the QM region via the effective point charges on the MM atoms. These methods, with or without such polarization, are termed electronic embedding (EE) and mechanical embedding (ME), respectively (*52*, *53*). The QM/MM calculations were carried out employing the ONIOM scheme as implemented in GAUSSIAN03 (*54*) using the AMBER force field (*55*) for the MM region. Our computational procedure is to take the appropriate crystal structure, solvate it with a large number (∼7500) of TIP3P (*56*) water molecules, and relax the protein using the AMBER force field augmented with the copper parameters developed by Comba and Remenyi (*57*). Thus, for native rusticyanin and

H143M, respectively (reported herein), the $[Cu(Im)_2(SCH_3)S(CH_3)_2]$ (Im = imidazole) and $[Cu(Im)(SCH_3)(S(CH_3)_2)_2]$ entity was the QM part of the QM/MM model and was described at the DFT level of theory. Here the cysteine, histidines, and methionine are partitioned as follows. Cysteine is terminated between C^β and C^α bonds (SCH_3); histidines and methionine are partitioned between C^γ and C^β bonds [Im and $S(CH_3)_2$]. For M148Q (PDB code 1E30), the axial glutamine is partitioned between C^β and C^α bonds ($NH_2COCH_2CH_3$). The QM/MM partitioning of rusticyanin and the two mutants is shown in Figure 1. All atoms in the QM region, together with some important MM residues, listed in Table 2, were optimized, while the remainder of the protein and solvating waters were held fixed.

In view of the problems of calculating absolute redox potentials, it is usual to compute the relative values for similar proteins (*18*) using simplified models in the hope that contributions such as entropy and other effects, for example, the differential solvation energy of the two oxidation states, will effectively cancel. In this paper we are mainly concerned with active site structures, and we wish to see if the trends in the redox potentials which accompany mutations can be predicted in terms of the measured and predicted structural changes at the active site. This could well be so, since no changes in the actual residues outside the active site have been made. We have calculated a number of energetic quantities related to the redox potential of the copper core. The vertical electron detachment and attachment energies (VDE, VAE) are the energy differences between the Cu(I) and Cu(II) species. The VDE is computed at the equilibrium geometry of the Cu(I) species and the VAE at the geometry of the Cu(II) species. The adiabatic electron detachment energy (ADE) is the difference between the energies of the Cu(I) and Cu(II) species, each at their equilibrium geometry. The one-electron oxidation reaction corresponds to the ADE which may thus be used as an estimate of the redox potential. The difference between the ADE and the VDE and VAE, respectively, gives the inner-sphere reorganization energy for the oxidized (λ_{ox}) and reduced states (λ_{red}), the total reorganization energy (λ_i) being the sum of these values.

RESULTS AND DISCUSSION

Spectroscopic and Redox Properties of the Proteins. In common with other type 1 Cu-containing proteins rusticyanin exhibits absorbance at 592 and 449 nm at a ratio of 2.08, with a further band at 700 nm. Rusticyanin has a rhombic EPR spectrum with $g_x = 2.015$, $g_y = 2.052$, $g_z = 2.211$, $A_x = 6.5$ mT, $A_y = 1.3$ mT, and $A_z = 5.0$ mT (*28*). As has been seen previously with other T1 Cu proteins (His117Gly in azurin etc.), the mutation of the surface-exposed His ligand resulted in a colorless protein. The H143M mutant exhibits only a single absorbance band at 280 nm arising from aromatic residues. No EPR-active species was detected, indicating that the protein was in the reduced state. Attempts to oxidize the protein using chemical methods (K_2IrCl_6) proved unsuccessful, suggesting that the potential could be in excess of 800 mV. XRF data (not shown) and EXAFS confirmed that Cu was present in the sample in the Cu(I) state.

Atomic Resolution Crystal Structures. The 1.27/1.1 Å resolution structures of native and H143M rusticyanin both contain 1 molecule in the $P2_1$ asymmetric unit and comprise 154/153 residues and 86/274 water molecules, respectively. The final crystallographic R/R_{free} factors were 12.0%/13.5% (native) and 14.0%/17.0% (H143M). The first residue at the N-terminus is disordered in both structures and has been omitted from the models, as is residue 2 in the H143M structure. The C-terminal Lys in the native structure is

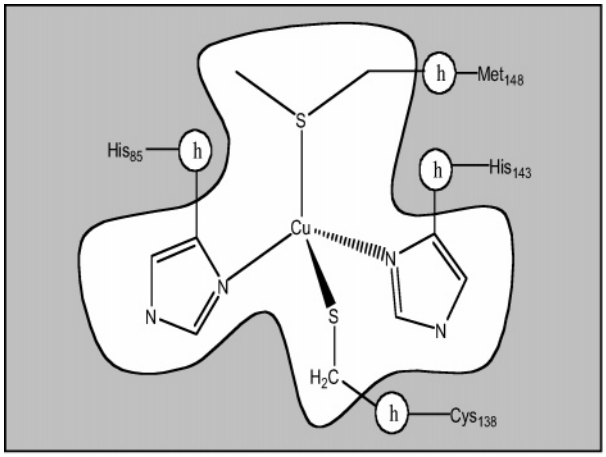

(a) Native rusticyanin

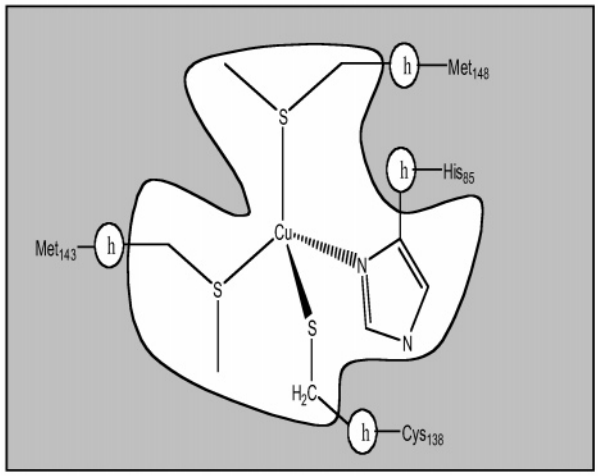

(b) His143Met mutant

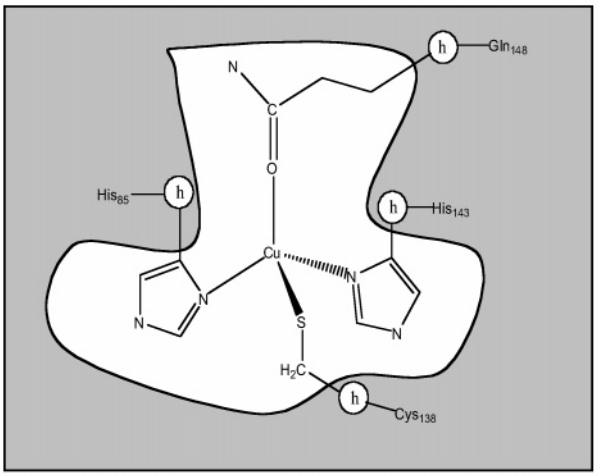

(c) Met148Gln mutant

FIGURE 1: QM/MM partitioning for (a) native rusticyanin, (b) the H143M mutant, and (c) the M148Q mutant.

Table 2: QM (in Bold) and MM Residues Optimized in QM/MM Calculations

system	amino acid residues
native Rc	Ala44, Val45, Phe51, Phe52, Ser53, Phe54, Asn80, Gly84, **His85**, Ser86, Phe111, Ser112, **Cys138**, Val137, Gln139, Ile140, Pro141, Gly142, **His143**, Ala144, **Met148**
H143M	Phe51, Pro52, Ser53, Phe54, Phe83, Gly84, **His85**, Ser86, **Cys138**, Val137, Gln139, Ile140, Pro141, Gly142, **Met143**, Ala144, **Met148**, Phe149
M148Q	Phe51, Pro52, Ser53, Phe54, Phe83, Gly84, **His85**, Ser86, **Cys138**, Gln139, Ile140, Pro141, Gly142, **His143**, Ala144, Ala145, Thr146, Gly147, **Gln148**
C138S	Ala44, Val45, Phe51, Phe52, Ser53, Phe54, Asn80, Gly84, **His85**, Ser86, Phe111, Ser112, **Ser138**, Val137, Gln139, Ile140, Pro141, Gly142, **His143**, Ala144, **Met148**

modeled in two conformations, while the side chain N^{ζ} atoms of residues 20 and 101 (native) and Lys25 and Lys36 (H143M) were not clear in the electron density and so were assigned an occupancy of zero. In the H143M model, the side chains of 10 residues were modeled in alternative conformations.

There are two structures of native rusticyanin at 1.9 Å (PDB code 1RCY; *6*) and 2.1 Å (PDB code 1A8Z; *7*) resolutions in the Protein Data Bank. The current structure of the native protein to 1.27 Å resolution thus represents a significant improvement in the quality of the structural information. The H143M mutant retains the overall structural features of native rusticyanin. Both fold as a Greek key β-sandwich core consisting of two β-sheets and the N-terminal extension, unique to rusticyanin, connected by several loops and coils. Superposition of the Cα atoms of the H143M structure with the native structure gives an RMS deviation of 0.25 Å. Although the overall RMS deviation is modest, there are significant differences between the H143M and native rusticyanin structures. Structural differences appear in the loop regions of 46−49, 114−119, and in particular the proline-rich loop 94−106. This loop packs against the β-turn and 3_{10}-helix which is responsible for providing the C-terminal cluster of Cu-coordinating residues (*6*). The side chain orientations of amino acids also show the most deviation in this area. Residue 93 is modeled as a Gly in H143M and Val in the 1.27 Å native structure. This has resulted from a deviation in the sequences of the wild-type protein and the recombinant proteins. The His143Met mutation also results in a positional difference of between 0.3 and 0.4 Å for the neighboring residues Pro141 and Gly142, which are located in a type II β-turn. The mean anisotropy values for the H143M and native Rc structures were calculated to be 0.48 and 0.43 for protein atoms and 0.50 and 0.35 for solvent atoms, respectively. This mean protein value is close to the average for protein structures at atomic resolution (*58*). In both cases the Cu atom has an anisotropy of ∼0.4. With the exception of a number of surface residues and small loop regions, the molecules did not exhibit significant anisotropy.

Native and H143M Cu Sites. The copper site of native rusticyanin in the 1.27 Å structure is similar to that reported previously at lower resolution (*6*, *7*) (Figure 2A, Table 3). Cu is coordinated by three strong ligands, His85 $N^{\delta 1}$, Cys138 S^{γ}, and His143 $N^{\delta 1}$, in a trigonal planar geometry and an axial ligand Met148 S^{δ}. The *B*-factors for the ligating atoms are between 11.5 and 13.1 $Å^2$, which compares well with that of the Cu atom at 13.4 $Å^2$. The Cu site is comparatively stable, as shown by anisotropic thermal probability ellipsoids (Figure 3A). Crystals of the native protein could only be obtained in the reduced, Cu(I) form. Tests with the chemical

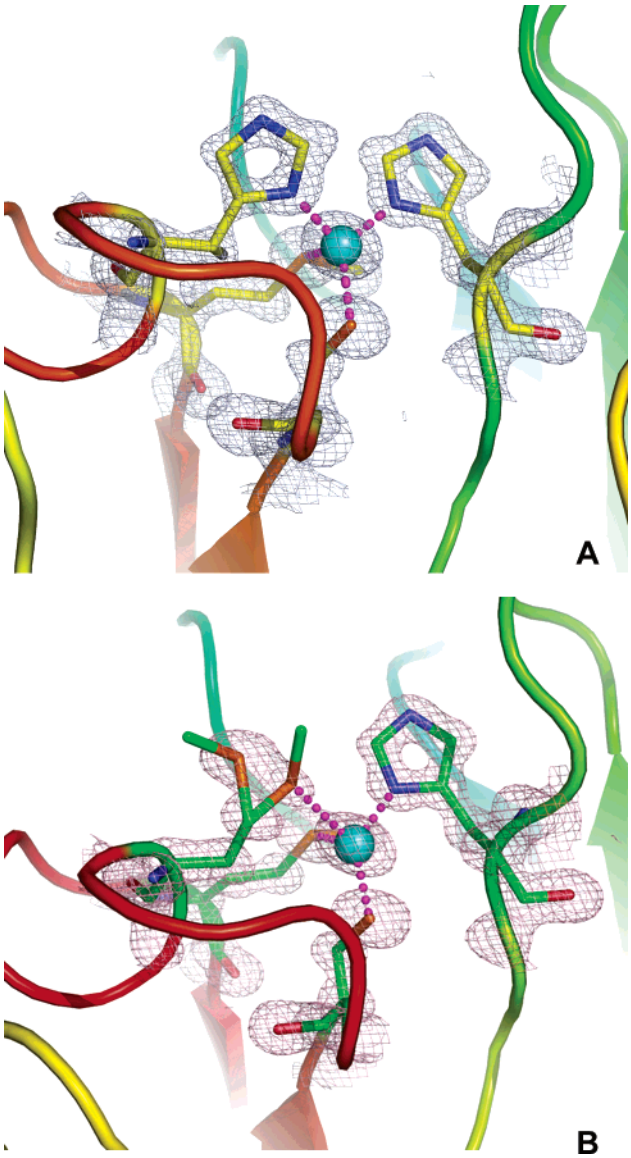

FIGURE 2: Active site electron density for (A) native and (B) H143M rusticyanin.

oxidant K_2IrCl_6 proved the crystals contained Cu and were redox-active; however, after treatment with the oxidant crystalline order was lost, possibly due to the formation of a heavy atom derivative. The comparatively long (2.23 Å) Cu−Cys138 S^{γ} distance is consistent with this oxidation state and is confirmed by EXAFS data on the oxidized and reduced states of the enzyme (Table 3). A superposition between the 1.27 and 1.9 Å structures is given in Figure 4A. In the 1.9 Å structure (*6*), a short (1.89 Å) Cu− His143 $N^{\delta 1}$ bond length was observed. It was suggested that this strong interaction might be in part responsible for the

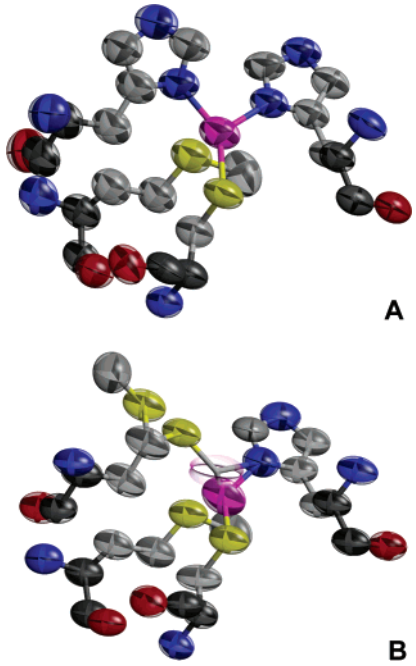

FIGURE 3: Anisotropic thermal probability ellipsoids for the active site and cupredoxin core of (A) native and (B) H143M rusticyanin. As expected, the core shows no significant areas of anisotropy in either structure whereas in the mutant structure the highly anisotropic nature of the closer sulfur position and methyl groups of the Met143 side chain can clearly be seen.

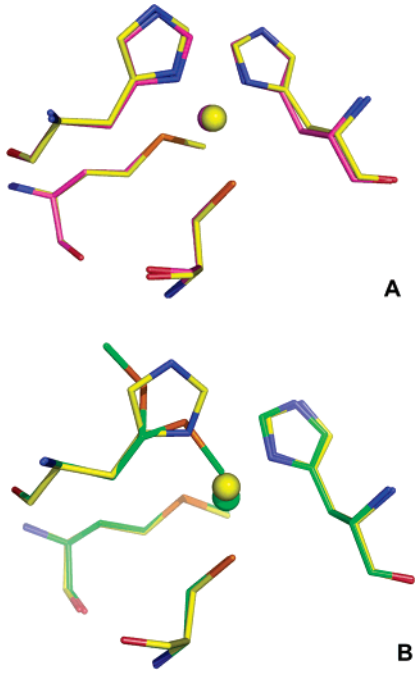

FIGURE 4: Least-squares superposition of the 1.27 Å rusticyanin Cu site (yellow) with (A) the previous 1.9 Å structure (magenta) and (B) the His143Met Cu site (green).

elevated redox potential of rusticyanin. The near-atomic resolution of the 1.27 Å structure allows these interpretations to be revisited. We observe a much more typical Cu−ligand bond length of 2.08 Å for Cu−His143 $N^{\delta 1}$. The Cu−Cys138 S^{γ} bond length is similar to that in the 1.9 Å structure. A 3D EXAFS simulation of the reduced protein is consistent with the Cu site depicted by the near-atomic resolution crystallographic data, with a Cu−His143 $N^{\delta 1}$ bond length of 2.02 Å (Table 3). The observation that the Cu center parameters are in fact fairly typical for cupredoxins suggests that the structural factors which lead to the unusually high redox potential of rusticyanin may lie outside of the first coordination sphere.

In the H143M structure, the side chain of the mutated Met143 residue has been modeled in two conformations with equal occupancies (Figure 2B). One sulfur atom is at 2.87 Å from Cu, thus forming a weak ligand interaction while the second sulfur position is too distant to interact at 4.24 Å from Cu. The temperature factor of the distant sulfur is 11.9 $Å^2$ compared to 15.1 $Å^2$ for the Cu atom. The closer sulfur atom has a *B*-factor of 21.1 $Å^2$, almost double that of the distant sulfur, indicating that the atom in this position is more disordered. The occupancies of the two sulfur positions were refined using the free-variable option in SHELX97 and are equivalent. The high anisotropy of the closer sulfur position is illustrated using 50% probability thermal ellipsoids (Figure 3B). Superposition of the H143M Cu site with that of the native protein (Figure 4B) shows close similarity except for a small (0.17 Å) movement of His85. The Cu position itself is shifted ~0.6 Å toward the two sulfurs of Cys138 and Met148. The His85 $N^{\delta 1}$−Cu−His(Met $S^{\delta 1}$)143 $N^{\delta 1}$ angle shows a decrease from 103° to 86° and 89° (the near and far sulfur positions, respectively) relative to the native protein. In addition, the Met148 S^{δ}−Cu−Cys138 S^{γ} angle is increased from 105° to 119°. In the H143M structure a half-occupancy solvent molecule has been modeled which

Table 3: Experimental Metal−Ligand Bond Lengths and Angles

	native Rc 1.27 Å (red)	native Rc 1.9 Å (red)	native Rc EXAFS (ox)	native Rc EXAFS (red)	H143M 1.1 Å (red)	3D EXAFS H143M (red)	EXAFS M148Q (ox)	EXAFS M148Q (red)	M148Q 1.5 Å (red)
bond length (Å)									
Cu−His85 $N^{\delta 1}$	2.06	2.04	2.05	2.12	1.89	1.94	1.95	1.92	1.98
Cu−His143 $N^{\delta 1}$	2.08	1.89	1.93	2.02			1.95	2.06	2.02
Cu−Met143 $S^{\delta 1}$					2.87, 4.24	2.88, 4.24			
Cu−Cys138 S^{γ}	2.23	2.26	2.16	2.21	2.14	2.15	2.15	2.20	2.18
Cu−Met148 S^{δ}	2.92	2.88	3.12	3.03	2.50	2.46			
Cu−Gln148 O								2.30	2.33
bond angle (deg)									
His85 $N^{\delta 1}$−Cu−Cys138 S^{γ}	126	128	126	125	133	133	118	119	119
His85 $N^{\delta 1}$−Cu−Met148 S^{δ}	86	85	86	86	96	96	97	96	96
His85 $N^{\delta 1}$−Cu−His(Met $S^{\delta 1}$)143 $N^{\delta 1}$	103	105	103	103	86, 89	86, 89	100	101	101
His(Met $S^{\delta 1}$)143 $N^{\delta 1}$−Cu−Cys138 S^{γ}	125	119	125	124	122, 121	122, 121	134	133	133
His(Met $S^{\delta 1}$)143 $N^{\delta 1}$−Cu−Met148 S^{δ}	101	106	101	101	90, 86	90, 86	95	93	93
Met(Gln148 O)148 S^{δ}−Cu−Cys138 S^{γ}	105	106	105	105	119	119	105	105	105

interacts with the closer conformation of Met143 and refines with a *B*-factor of 24.6 Å^2 compared to 21.1 Å^2 for the corresponding sulfur of the methionine. Thus this water is in this position when the sulfur atom is nearer the Cu atom. This surface water is in turn weakly bonded (3.5 Å) to a number of other solvent molecules. When Met143 S$^{\delta}$ is in its more distant position (more ordered), the Cu site adopts a 3-coordinate geometry.

The replacement of the His143 ligand with a Met has a relatively small effect on the collection of hydrophobic residues that are in the vicinity of the usual His143 residue and the Cu site. The outward flipping of the distant position of the Met143 side chain away from Cu results in small changes in the positions of Phe51, Pro52, Phe111, and Ile140. The Ile140 C$^{\gamma}$ position is essentially the same and maintains its close position to the Cu atom. The largest change occurs in the Phe83 position where the ring is rotated by ~20° in the direction of the Cu atom and has also moved closer to the Cu by some 0.8 Å.

Solvent Structure. In the native structure of rusticyanin at 1.9 Å (PDB code 1RCY) a total of 128 solvent molecules were modeled; this is considerably more than in the native structure presented here. This apparent discrepancy could be due to dehydration of the crystal used for native data collection as a result of prolonged X-ray exposure at room temperature. In contrast, the H143M structure with similar unit cell dimensions has a total of 274 solvent molecules. In the H143M structure the side chain of Gln139 which is adjacent to the Cu ligand Cys138 is now seen to be bonded to a solvent molecule, Wat2285, which is observed to be involved with an outer Cu-sphere hydrogen-bonding network. In both the native (1.27 and 1.9 Å) and His143Met structures, two solvent molecules (Wat2002 and Wat2004) are involved in hydrogen bonding, helping to stabilize the main chain carbonyl atoms of Cys138 and Ile140 along with Ala144, Val98, and Ala99. The observation of these solvent molecules in the lower resolution structures is consistent with them exhibiting among the lowest *B*-factors of all solvent molecules in the current structures. Residues Val98 and Ala99 are located in the hydrophobic proline-rich loop that forms a close interaction with the β-turn and the 3_{10}-helix which provide the C-terminal cluster of Cu residues (*6*). It would be tempting to suggest that this close interaction of the loop brings the backbone atoms of Val98 and Ala99 into a position to form a tight hydrogen-bonding arrangement, ideal for holding solvent molecules. It is possible that this is a structural arrangement that exists in order to prevent the hydrolysis of the Cu ligand, Cys138.

EXAFS Data and Comparison with Crystal Structures. Cu K-edge EXAFS data for native and M148Q rusticyanin in solution at 100 K were collected for both the oxidized and reduced forms of the proteins. For H143M, data were collected only for the reduced form. Data were analyzed with the crystal structure coordinates, using the 3D EXAFS refinement method (*59*). The use of this method of refinement in providing metrical accuracy for metal−ligand stereochemistry using crystallographic coordinates has recently been highlighted in the case of the copper nitrite reductase (*60*) and MoFe nitrogenase proteins (*61*). EXAFS-derived values for copper−ligand bond distances are given in Table 3.

For reduced native rusticyanin, the Cu−Cys138 S$^{\gamma}$ distance is 2.21 Å, compared to 2.16 Å in the oxidized protein,

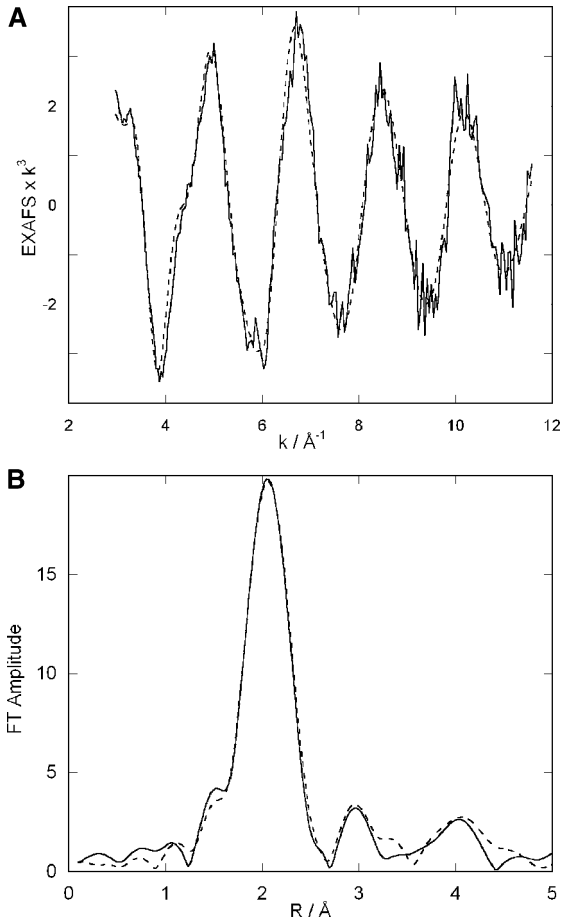

FIGURE 5: Simulation (dashed line) of the (A) k^3-weighted Cu K edge EXAFS data for H143M using 1.1 Å crystal coordinates and (B) the corresponding Fourier transforms.

confirming that the crystallographic structures reported here are for the reduced state. There is also an overall increase in the Cu−histidine distances (by 0.05 Å) in going from oxidized to reduced copper. The position of the Met148 ligand is less well defined because its contribution to the EXAFS data is much weaker than for the other ligands.

For reduced H143M, a close agreement between the 3D EXAFS results and the 1.1 Å crystallographic structure is clearly evident (Figure 5, Table 3). The Cys138 S$^{\gamma}$−Cu and Met143 S$^{\delta 1}$−Cu distances are within 0.01 Å of their values in the crystal structure where the Met143 S$^{\delta 1}$−Cu distance of the more distant sulfur atom is identical at 4.24 Å.[3] Both sulfur positions of the mutated Met143 side chain were accounted for during 3D EXAFS refinement. The Cu−His85 N$^{\delta 1}$ distance is slightly longer at 1.94 Å compared to 1.89 Å in the crystal structure whereas the Cu−Met148 S$^{\delta}$ distance is shorter by 0.04 Å at 2.46 Å compared to the crystallographic value of 2.50 Å.

EXAFS-derived distances for the copper−ligand bond lengths in M148Q rusticyanin are also given in Table 3. The crystal structure of M148Q was previously determined to 1.5 Å resolution (*15*), and this was used as the starting model for 3D EXAFS refinement. The EXAFS data show reasonable agreement with the crystal structure for the three equatorial ligands. A 0.03 Å reduction in the Cu−His85 N$^{\delta 1}$

[3] Such a distance would not have been incorporated in XAFS refinement without the crystallographic information.

Table 4: Structures of Isolated (Gas Phase) and Embedded Cluster Models of Reduced Rusticyanin, the H143M Mutant, and the Met148Q Mutant

	native Rc				H143M				M148Q			
	X-ray[a]	gas phase	QM/MM (EE)	QM/MM (ME)	X-ray[a]	gas phase	QM/MM (EE)	QM/MM (ME)	X-ray[b,c]	gas phase	QM/MM (EE)	QM/MM (ME)
bond length (Å)												
Cu−His85 $N^{\delta1}$	2.06	2.13	2.13	2.12	1.89	2.12	1.96	2.01	1.98 (2.2)	2.04	2.11	2.09
Cu−His(Met $S^{\delta1}$)143 $N^{\delta1}$	2.08	2.07	2.18	2.22	4.24	2.45	4.73	4.59	2.02 (2.1)	2.10	2.08	2.07
Cu−Cys138 S^{γ}	2.23	2.27	2.23	2.24	2.14	2.29	2.16	2.18	2.18 (2.3)	2.21	2.23	2.24
Cu−Met(Gln O)148 $S^{\delta1}$	2.92	2.54	2.74	2.51	2.50	2.67	2.41	2.30	2.33 (2.5)	3.49	2.42	2.47
bond angle (deg)												
His85 $N^{\delta1}$−Cu−Cys138 S^{γ}	126	108	127	123	134	106	147	131	119 (132)	133	124	124
His85 $N^{\delta1}$−Cu−Met(Gln O)148 S^{δ}	86	100	85	90	96	104	89	81	96 (88)	79	87	87
His85 $N^{\delta1}$−Cu−His(Met $S^{\delta1}$)143 $N^{\delta1}$	103	114	95	95	89	105	80	81	101 (98)	104	107	108
His(Met $S^{\delta1}$)143 $N^{\delta1}$−Cu−Cys138 S^{γ}	125	124	127	120	121	106	120	116	133 (125)	122	124	122
His(Met $S^{\delta1}$)143 $N^{\delta1}$−Cu−Met148(Gln O) S^{δ}	101	103	100	105	86	115	81	87	93 (91)	81	92	91
Met(Gln O)148 S^{δ}−Cu−Cys138 S^{γ}	105	105	113	119	119	120	118	128	105 (110)	101	112	114

[a] Denotes X-ray structures reported herein. [b] X-ray structure of M148Q (1E30). [c] Denotes structure (in parentheses) of reduced stellacyanin (1X9U).

Table 5: Structures of Isolated (Gas Phase) and Embedded Cluster Models of Oxidized Rusticyanin, the H143M Mutant, and the M148Q Mutant

	native Rc				H143M			M148Q			
	EXAFS[a]	gas phase	QM/MM (EE)	QM/MM (ME)	gas phase	QM/MM (EE)	QM/MM (ME)	X-ray[b]	gas phase	QM/MM (EE)	QM/MM (ME)
bond length (Å)											
Cu−His85 $N^{\delta1}$	2.05	2.09	2.02	2.02	2.01	2.00	2.00	2.02	2.04	1.99	2.00
Cu−His(Met $S^{\delta1}$)143 $N^{\delta1}$	1.93	2.02	2.06	2.11	2.50	2.45	2.51	1.98	2.03	2.03	2.02
Cu−Cys138 S^{γ}	2.16	2.17	2.16	2.17	2.16	2.16	2.17	2.18	2.24	2.16	2.18
Cu−Met(Gln O)148 $S^{\delta1}$	3.12	2.42	2.72	2.53	2.40	2.45	2.38	2.34	2.01	2.14	2.20
bond angle (deg)											
His85 $N^{\delta1}$−Cu−Cys138 S^{γ}	126	100	135	141	138	142	139	133	95	136	130
His85 $N^{\delta1}$−Cu−Met(Gln O)148 S^{δ}	86	104	87	90	99	89	94	93	141	97	94
His85 $N^{\delta1}$−Cu−His(Met $S^{\delta1}$)143 $N^{\delta1}$	103	100	99	98	100	91	90	101	94	99	105
His(Met $S^{\delta1}$)143 $N^{\delta1}$−Cu−Cys138 S^{γ}	125	139	114	100	99	111	102	119	151	119	122
His(Met $S^{\delta1}$)143 $N^{\delta1}$−Cu−Met148(Gln O) S^{δ}	101	98	105	108	102	100	102	96	89	102	98
Met(Gln O)148 S^{δ}−Cu−Cys138 S^{γ}	105	111	111	116	113	116	121	105	102	97	99

[a] Denotes the EXAFS structure (reported here). [b] Denotes the X-ray structure (1X9R, oxidized stellacyanin).

bond length and increases of 0.11 and 0.05 Å in the Cu−His143 $N^{\delta1}$ and Cu−Cys138 S^{γ} distances occur between the Cu(II) and Cu(I) states. The axial Gln148 O in the reduced protein is some 2.3 Å from Cu. In the oxidized M148Q protein, Gln148 did not contribute significantly to the EXAFS spectrum, indicating that it had moved significantly further away from Cu and/or become disordered.

In our previous 1.5 Å crystal structure of the M148Q mutant, the protein was assessed to be in the oxidized state on the basis of the blue color of the crystal prior to data collection. The structure showed a Cu−Gln148 O distance of 2.33 Å. In light of the EXAFS data presented here, it appears likely that photoreduction of the crystal had taken place during X-ray data collection and that the structure was in fact that of Cu(I)−M148Q.

COMPUTATIONAL RESULTS

Cluster Studies. We first describe the predicted structures and redox properties of the three proteins given by the isolated cluster, namely, the gas-phase model. In the Cu(I) state, the three clusters have a trigonal structure with Cu−ligand bond lengths which vary upon mutation (Table 4). The M148Q mutant has a long Cu−Gln148 O bond length (3.49 Å), whereas the corresponding length (Cu−Met148 S^{δ}, 2.54 Å) in the native protein is predicted to be considerably shorter, an effect reflected in the shorter Cu−Cys138 S^{γ} distance (2.21 Å), compared to the value in the native protein (2.27 Å). Mutation of an equatorial histidine ligand of rusticyanin by methionine (H143M) has little effect on the bond lengths involving the remaining two equatorial ligands. In this mutant the equatorial methionine (M143) has a long Cu−S bond (2.45 Å), and this value for the axial methionine, M148 (2.67 Å), is somewhat longer than that in the native protein. The inadequacy of isolated cluster models for predicting the Cu−ligand coordination in the actual protein is highlighted by a comparison with our structural data for the Cu(I) state of the H143M mutant, where the Cu−Met143 $S^{\delta1}$ distance is in error by nearly 2 Å (Table 4). There is a similar discrepancy between the experimental structure of reduced M148Q and our cluster geometry where the measured Cu−Gln148 O distance is ~1 Å shorter than the predicted value.

The structures of the Cu(II) states as described by the cluster model (Table 5) are tetragonal with bond lengths which are generally shorter than those for the Cu(I) states, which is particularly evident for the methionine and glutamine ligands. In the axial M148Q mutant the short Cu−Gln148 O bond (2.01 Å) leads to a longer Cu−Cys138 S^{γ} bond (2.24

Table 6: Vertical Detachment and Attachment Energy (VDE, VAE), Adiabatic Detachment Energy (ADE), and Reorganization Energy (λ) (kcal mol^{-1}) of Native Rusticyanin and the H143M, M148Q, and C138S Mutants

	VDE	VAE	ADE	λ_{ox}	λ_{red}	λ_i
gas phase						
native Rc	129.5	112.0	119.5	10.0	7.5	17.5
H143M	138.2	121.7	128.2	10.0	6.5	16.6
M148Q	142.5	97.8	116.0	26.5	18.2	44.7
C138S	124.5	96.9	111.8	12.7	14.9	27.6
QM/MM (EE)						
native Rc	119.5	111.9	115.6	3.9	3.7	7.6
H143M	144.2	121.5	125.7	18.5	4.2	22.7
M148Q	117.1	100.7	113.7	3.4	13.0	16.4
C138S	141.5	98.0	109.4	32.1	11.4	43.4
QM/MM (ME)						
native Rc	120.4	111.9	116.2	4.2	4.3	8.5
H143M	143.1	122.3	126.1	17.0	3.8	20.8
M148Q	118.2	103.0	113.9	4.3	10.9	15.2
C138S	141.4	98.1	109.5	31.9	11.4	43.3

Table 7: Relative Reduction Potentials (mV)

protein	experiment	gas phase	QM/MM (EE)	QM/MM (ME)
native Rc	0	0	0	0
H143M	n/a	+379	+438	+429
M148Q	−117	−152	−81	−101
C138S	n/a	−334	−269	−291

Å), whereas in the equatorial H143M mutant replacing a strongly bound histidine with a methionine leads to a short Cu−Cys138 S$^{\gamma}$ bond (2.16 Å). A similar effect has been noted by others for stellacyanin and rusticyanin (*30*).

These differences in the geometric structure of the active site between the Cu(I) and Cu(II) species are clearly central to understanding the effect that mutations have on the redox properties. The reorganization energies (Table 6), λ_i, which are also central to understanding the rate of electron transfer, are particularly large for the cluster model, due to the lack of the geometric constraints of the protein (entatic effect) (*21*). The large value for the M148Q mutant (44.7 kcal mol^{-1}) reflects the considerable reduction in the axial bond length occurring upon oxidation.

For the other two proteins (native and H143M) the values of λ_i are still substantial but are quite similar in magnitude (17.5 and 16.6 kcal mol^{-1}). Despite the lack of the protein environment, the order of the redox potentials compared to the native protein is correctly given by the cluster calculations (Table 7). The large reorganization energy of the Met148Q mutant is responsible for this protein having the smallest redox potential of all three, despite it having the largest vertical ionization energy. It is of interest that the reorganization energy for the native protein and H143M mutant is very similar for the cluster model. Thus, the difference in the redox potentials for these two proteins is found in the vertical ionization energies. This can be attributed to the hardness of the histidine ligand compared to methionine, where the higher oxidation state is stabilized by the large nitrogen negative charge. Thus, the isolated cluster calculations have shown a number of important effects, both structural and energetic, arising from mutation. Of course, isolated clusters cannot differentiate the two conformers of H143M evident in the crystal structure and the effect of the protein backbone. We now examine how these effects are modified by the protein, by describing the predictions of the hybrid QM/MM calculations.

QM/MM Studies. We now consider the predictions of the active site structure and first focus on the M148Q mutant where there are EXAFS data for both oxidation states and X-ray data for the reduced protein. For comparison with our calculated structures, we also take the X-ray data for the reduced and oxidized state of stellacyanin (Tables 3−5). The major change from the cluster model is for the Cu−Gln148 O bond length, which has increased by 0.1−0.2 Å in the oxidized state and decreased by ∼1 Å in the Cu(I) state. The actual bond length predicted for the reduced state (∼2.42 Å) is now close to the experimental value of ∼2.30 Å (Table 4). The predicted axial bond length is 2.14 Å in the Cu(II) species, whereas in the EXAFS data the axial ligand did not contribute to the EXAFS spectrum, suggesting that the bond length had increased significantly and/or that the ligand had become disordered. Previous EXAFS studies on the Cu coordination site in *Rhus vernicifera* stellacyanin (*62*), carried out at pH 6.4, showed a similar behavior, with an increase of the Cu−Gln O distance from 2.45 Å in the reduced protein to 2.7 Å in the oxidized protein. The predicted Cu−Cys138 S$^{\gamma}$ lengths of 2.3 and 2.16 Å for the reduced and oxidized states, respectively, are in good agreement with the experimental values of 2.3 and 2.18 Å, respectively, as are the Cu−His85(143) N$^{\delta 1}$ distances.

For the H143M mutant our 1.1 Å X-ray data for the reduced state have suggested that the equatorial methionine may occupy two different positions (2.87 and 4.24 Å, Table 3). For QM/MM calculation, we started with each of these two possibilities for our optimization procedure. We find that both give the same optimized structure for the reduced state (Table 4) which shows a long Cu−Met143 S$^{\delta 1}$ distance (4.73 Å) and correspondingly short Cu−Cys138 S$^{\gamma}$ (2.16 Å) and Cu−His85 N$^{\delta 1}$ distances (1.96 Å). There is some difference in the Cu−His85 N$^{\delta 1}$ distance given by EXAFS and the 1.1 Å crystal structure (Table 3). Our predicted value (1.96 Å) is closer to the EXAFS value (1.94 Å). For the remaining copper−ligand distances, except for the long Cu−M143 S$^{\delta 1}$ distance, there is good agreement with the 1.1 Å crystal data. The calculated Cu−M143 S distance (4.73 Å) departs from the experimental values obtained from the crystal structure and EXAFS data, both being 4.24 Å. The observation of only the distal Cu−M143 S in the calculations together with the higher *B*-factor for the proximal position of M143S and greater anisotropy in the 1.1 Å structure suggests that the closer conformer is unstable when the protein is reduced. It is thus likely that the distant M143S in the experimental structure has an occupancy higher than 50% as is reflected by its low *B*-value compared to the Cu atom.

In the case of native rusticyanin, when compared to our 1.27 Å structure of the reduced protein, the QM/MM model yields reasonably accurate bond lengths for Cu−His85 N$^{\delta 1}$ (Tables 4 and 5), while the Cu−His143 N$^{\delta 1}$ length is a little overestimated (∼0.1 Å), and the Cu−Cys138 S$^{\gamma}$ length is excellently reproduced (2.23 Å). It is interesting to note that we find the long Cu−Met148 S$^{\delta}$ bond to be rather sensitive to the QM/MM model used. In the EE method, this distance is 2.74 Å, about 0.2 Å longer than that found by the ME method (2.51 Å). This reflects the relatively shallow potential energy curve for this weakly bound ligand in this case. However, both of these values are shorter than the experimental value (2.92 Å). We again find that the largest

Table 8: Structures of Isolated (Gas Phase) and Embedded Cluster Models of the Reduced and Oxidized Forms of the C138S Mutant of Rusticyanin

	reduced			oxidized		
	gas phase	QM/MM (EE)	QM/MM (ME)	gas phase	QM/MM (EE)	QM/MM (ME)
bond length (Å)						
Cu−His85 $N^{\delta 1}$	2.08	1.90	1.92	2.07	2.04	2.04
Cu−His143 $N^{\delta 1}$	2.03	4.06	3.92	2.01	2.12	2.15
Cu−Ser138 O^{γ}	2.03	1.80	1.82	1.80	1.80	1.81
Cu−Met148 $S^{\delta 1}$	2.49	3.19	3.14	2.42	2.52	2.48
bond angle (deg)						
His85 $N^{\delta 1}$−Cu−Ser138 O^{γ}	97	175	173	92	151	155
His85 $N^{\delta 1}$−Cu−His143 $N^{\delta 1}$	128	74	77	98	94	93
His85 $N^{\delta 1}$−Cu−Met148 S^{δ}	107	80	80	115	88	88
Ser138 O^{γ}−Cu−His143 $N^{\delta 1}$	116	109	100	149	102	97
Ser138 O^{γ}−Cu−Met148 S^{δ}	92	104	105	105	109	110
His143 $N^{\delta 1}$−Cu−Met148 S^{δ}	110	71	74	98	111	110

bond length change on switching from the isolated cluster to the QM/MM model is for the Cu−Met148 S^{δ} interaction.

In the comparison of our structures predicted by the QM/MM model with new structural data described herein (Tables 3−5) and with some published data, we see there is generally quite good agreement, but not at the level found for a similar comparison for small gas-phase species. It may be that, in contrast to small gas-phase species, the potential energy surface for the protein is quite shallow in some regions. Thus, an alternative way of judging our predicted structures is to compare their energy with that of the corresponding cluster excised from the crystal data. To do this, we have first optimized the positions of the hydrogen atoms in the X-ray structure at the QM level. For the reduced state of the M148Q mutant, the two structures are within ~8 kcal mol^{-1}. This value is decreased to ~3 kcal mol^{-1} for the reduced state of the native protein and is ~ 9 kcal mol^{-1} for the reduced state of the H143M mutant.

Prediction of the Oxidized Cu Site of the H143M Mutant. We have previously found that the H143M mutant was not oxidized by K_2IrCl_6, and experimental data are thus available only for the reduced state. We have used the QM/MM model to predict the structure of the oxidized state. We find that when we start with the two conformers found experimentally, two corresponding oxidized structures are obtained. We here report the lower energy structure (by 13 kcal mol^{-1}), which has the shorter Cu−Met143 $S^{\delta 1}$ length. We find that the major change in the structure of the oxidized compared to the reduced state is a considerable reduction in the Cu−Met143 $S^{\delta 1}$ length, the other metal−ligand lengths being largely unchanged (Table 5).

Prediction of Redox Properties. We now consider the prediction of the ionization energies of the three proteins given by the QM/MM model. We have previously discussed their prediction by the cluster model. The generally smaller changes in the bond lengths between the Cu(I) and Cu(II) species found for the QM/MM compared to the cluster models, for the native protein and axial mutant, lead to correspondingly smaller inner-sphere reorganization energies (Table 6). The reverse is found for the equatorial mutant where the larger bond length change for the equatorial methionine leads to a somewhat larger reorganization energy. As far as the actual redox potentials are concerned, the experimental order which was correctly given by the cluster model is again given by the QM/MM model (Table 7), the M148Q mutant having the smallest redox potential and the actual relative values being little changed from those given by the isolated cluster.

Mutation of cysteine residues to serine has been much studied, particularly for iron−sulfur electron transfer proteins such as rubredoxins (*63*, *64*). In view of the large structural and energetic effects that we find for the equatorial mutation studied here (H143M), it is of interest to examine computationally the effect of mutating the equatorial cysteine to serine in the native rusticyanin (C138S). Both isolated and embedded cluster calculations were performed for this theoretical mutant (Table 8). The isolated cluster model predicts a 4-coordinate species for both the oxidized and reduced state, which is similar to H143M. However, in the QM/MM model the oxidized form remains tetracoordinate, as in the native protein, but there is extreme distortion of the reduced form. The axial methionine (Met148) and equatorial histidine (His143) are dissociated, giving an essentially linear 2-coordinate structure in the QM/MM model. As in the case of rubredoxins (*65*), the substitution of oxygen for sulfur leads to a preferential stabilization of the oxidized form and a smaller ADE for C138S compared to native rusticyanin (109.5 compared to 116.2 kcal mol^{-1}, Table 6). However, the large structural changes occurring upon ionization lead to the largest predicted reorganization energy (43.3 kcal mol^{-1}, Table 6) of the four rusticyanins studied here, which must militate against electron transfer. The corresponding redox potential is calculated to be ~290 mV lower than for native rusticyanin (Table 7) and is thus predicted to be the lowest in the family of cupredoxins. These predictions have yet to be tested experimentally.

CONCLUSIONS

The crystal structures of native rusticyanin, a cupredoxin with extreme properties, and of its redox-switch ligand mutant, H143M rusticyanin, have been solved to 1.27 and 1.1 Å, respectively. The metrical accuracy of the 1.27 Å native rusticyanin structure shows that, contrary to the earlier 1.9 Å structure of this protein, the Cu−His143 N^{δ} and Cu−Cys138 S^{γ} distances and the His85−Cu−Cys138 angle are typical to those observed in other cupredoxins, and, as such, these features in themselves are not responsible for the unusual redox properties of this cupredoxin. Thus, the high redox potential of rusticyanin must arise from structural elements outside the first coordination sphere. The 1.1 Å atomic resolution H143M structure yields very similar

metal−ligand bond distances to those determined by EXAFS data, highlighting the importance of atomic resolution structure determination for accurate structural information. EXAFS data for the M148Q mutant show that the axial Gln ligand is lost from the first coordination shell on oxidation of Cu. This indicates that the previously determined crystal structure of this mutant was in fact that of the reduced protein, rather than the oxidized state as had been thought.

The calculated (QM/MM) active site structures for the native and mutant proteins are in good agreement with the high-resolution experimental data, particularly when the complexity of the systems being studied is considered. We note that the two variants of the embedding models which we have considered lead to very similar quantitative conclusions. These calculations have allowed a model to be determined for the experimentally inaccessible Cu(II) state of the H143M mutant. Calculations based on the computed structures correctly predict the experimentally observed order of redox potentials: H143M > native > M148Q. The calculated redox potential of H143M (∼400 mV greater than rusticyanin) is consistent with the failure of chemical oxidants to restore a Cu(II) species of this mutant. Furthermore, we find that this equatorial mutant has a considerably greater reorganization energy than the native protein and also a somewhat greater value than the axial mutant (M148Q). This strongly suggests that electron transfer will be unfavorable in H143M. Our calculations on a C138S mutant, as yet not studied experimentally, suggest a low redox potential, but a large inner-sphere reorganization energy, suggesting that electron transfer could again be unfavorable.

An interesting outcome of the combination of theoretical and atomic resolution experimental data has been in the case of the H143M structure where many double conformations including that of the mutated residue have been observed. Calculations suggest that in the reduced form only the distal conformer is stable, which in fact turns out to be consistent with the high *B*-value and greater anisotropy for the proximal position. With increased availability of atomic resolution structural information, it should become possible to use these in conjunction with the theoretical approaches to provide additional structure−function information as well as shed light on intractable redox states as was the case here for the oxidized form of H143M.

ACKNOWLEDGMENT

We thank Dr. W. J. Ingledew for the gift of rusticyanin, CCLRC Daresbury Laboratory for access to synchrotron beamtime, and members of the Molecular Biophysics and Protein Crystallography groups at Daresbury for support and suggestions.

REFERENCES

1. Ronk, M., and Shively, J. E. (1991) Amino acid sequence of the blue copper protein rusticyanin from *Thiobacillus ferrooxidans*, *Biochemistry 30*, 9435−9442.
2. Kondrat'eva, T. F., Ageeva, S. N., Muntyan, L. N., Pivovarova, T. A., and Karavaiko, G. I. (2002) Strain polymorphism of the plasmid profiles in *Acidithiobacillus ferrooxidans*, *Microbiology 71*, 319−325.
3. Blake, R. C., and Shute, E. A. (1987) Respiratory enzymes in thiobacillus ferrooxidans−a kinetic study of electron transfer between iron and rusticyanin in sulfate media, *J. Biol. Chem. 262*, 14983−4989.
4. Ingledew, W. J., and Cobley, J. G. (1980) A potentiometric and kinetic study on the respiratory chain of ferrous iron grown *Thiobacillus ferrooxidans*, *Biochim. Biophys. Acta 590*, 141−148.
5. Blake, R., White, K. J., and Shute, E. A. (1996) Mixed-ligand complexes of iron with cyanide and phenanthroline as new probes of metalloprotein electron-transfer reactivity−analysis of reactions involving rusticyanin from *Thiobacillus ferrooxidans*, *J. Biol. Chem. 266*, 19203−19211.
6. Walter, R. L., Ealick, S. E., Friedman, A. M., Blake, R. C., Proctor, P., and Shoham, M. (1996) Multiple wavelength anomalous diffraction (MAD) crystal structure of rusticyanin: A highly oxidizing cupredoxin with extreme acid stability, *J. Mol. Biol. 263*, 730−751.
7. Harvey, I., Hao, Q., Duke, E. M. H., Ingledew, W. J., and Hasnain, S. S. (1998) Structure determination of a 16.8 kDa copper protein at 2.1 angstrom resolution using anomalous scattering data with direct methods, *Acta Crystallogr., Sect. D 54*, 629−635.
8. Botuyan, M. V., Toypalmer, A., Chung, J., Blake, R. C., Beroza, P., Case, D. A., and Dyson, H. J. (1996) NMR solution structure of Cu(I) rusticyanin from *Thiobacillus ferrooxidans*: Structural basis for the extreme acid stability and redox potential, *J. Mol. Biol. 263*, 752−767.
9. Grossmann, J. G., Ingledew, W. J., Harvey, I., Strange, R. W., and Hasnain, S. S. (1995) X-ray absorption studies and homology modelling define the structural features that specify the nature of the copper site in rusticyanin, *Biochemistry 34*, 8406−8414.
10. Hall, J. F., Kanbi, L. D., Harvey, I., Murphy, L. M., and Hasnain, S. S. (1998) Modulating the redox potential and acid stability of rusticyanin by site-directed mutagenesis of Ser86, *Biochemistry 37*, 11451−11458.
11. Kanbi, L. D., Antonyuk, S., Hough, M. A., Hall, J. F., Dodd, F. E., and Hasnain, S. S. (2002) Crystal structures of the Met148Leu and Ser86Asp mutants of rusticyanin from *Thiobacillus ferrooxidans*: Insights into the structural relationship with the cupredoxins and the multi copper proteins, *J. Mol. Biol. 320*, 263−275.
12. Guidici-Orticoni, M. T., Guerlesquin, F., Bruschi, M., and Nitschke, W. (1999). Interaction-induced redox switch in the electron-transfer complex rusticyanin-cytochrome *c*(4), *J. Biol. Chem. 274*, 30365−30369.
13. Nar, H., Messerschmidt, A., Huber, R., van de Kamp, M., and Canters, G. W. (1991) X-ray crystal structure of the 2 site specific mutants His35Gln and His35Leu of azurin from *Pseudomonas aeruginosa*, *J. Mol. Biol. 218*, 427−447.
14. Dodd, F. E., Hasnain, S. S., Abraham, Z. H. L., Eady, R. R., and Smith, B. E. (1995) Structure of a new azurin from the denitrifying bacterium *Alcaligenes xylosoxidans* at high resolution, *Acta Crystallogr., Sect. D 51*, 1052−1064.
15. Hough, M. A., Hall, J. F., Kanbi, L. D., and Hasnain, S. S. (2001) Structure of the M148Q mutant of rusticyanin at 1.5 angstrom: a model for the copper site of stellacyanin, *Acta Crystallogr., Sect. D 57*, 355−360.
16. Jeuken, L. J. C., van Vliet, P., Verbeet, M. P., Camba, R., McEvoy, J. P., Armstrong, F. K., and Canters, G. W. (2000) Role of the surface-exposed and copper-coordinating histidine in blue copper proteins: The electron-transfer and redox-coupled ligand binding properties of His117Gly azurin, *J. Am. Chem. Soc. 122*, 12186−12194.
17. Prudencio, M., Sawers, G., Fairhurst, S. A., Yousafzai, F. K., and Eady, R. R. (2002) *Alcaligenes xylosoxidans* dissimilatory nitrite reductase: Alanine substitution of the surface-exposed histidine 139 ligand of the type 1 copper center prevents electron transfer to the catalytic center, *Biochemistry 41*, 3430−3438.
18. Li, H., Webb, S. P., Ivanic, J., and Jensen, J. H. (2004) Determinants of the relative reduction potentials of type-1 copper sites in proteins, *J. Am. Chem. Soc. 126*, 8010−8019.
19. Datta, S. N., Sudhamsu, J., and Pandey, A. (2004) Theoretical determination of the standard reduction potential of plastocyanin in vitro, *J. Phys. Chem. 108*, 8007−8016.
20. De Rienzo, F., Gabdoulline, R. R., Wade, R. C., Sola, M., and Menziani, M. C. (2004) Computational approaches to structural and functional analysis of plastocyanin and other blue copper proteins, *Cell. Mol. Life Sci. 61*, 1123−1142.
21. Gray, H. B., Malmstrom, B. G., and Williams, R. J. P. (2000) Copper coordination in blue proteins, *J. Biol. Inorg. Chem. 5*, 551−559.
22. Koch, M., Velarde, M., Harrison, M. D., Echt, S., Fischer, M., Messerschmidt, A., and Dennison, C. (2005) Crystal structures of oxidized and reduced stellacyanin from horseradish roots, *J. Am. Chem. Soc. 127*, 158−166.

23. Dodd, F. E., Abraham, Z. H. L., Eady, R. R., and Hasnain, S. S. (2000) Structures of oxidized and reduced azurin II from *Alcaligenes xylosoxidans* at 1.75 angstrom resolution, *Acta Crystallogr., Sect. D 56*, 690−696.
24. Hwang, H. J., Berry, S. M., Nilges, M. J., and Lu, Y. (2005) Axial methionine has much less influence on reduction potentials in a Cu-A center than in a blue copper center, *J. Am. Chem. Soc. 127*, 7274−7275.
25. Solomon, E. I., Szilagyi, R. K., DeBeer, S. G., and Basumallick, L. (2004) Electronic structures of metal sites in proteins and models: Contributions to function in blue copper proteins, *Chem. Rev. 104*, 419−458.
26. George, S. D., Basumallick, L., Szilagyi, R. K., Randall, D. W., Hill, M. G., Nersissian, A. M., Valentine. J. S., Hedman B., Hodgson, K. O., and Solomon, E. I. (2003) Spectroscopic investigation of stellacyanin mutants: Axial ligand interactions at the blue copper site, *J. Am. Chem. Soc. 125*, 11314−11328.
27. Guckert, J. A., Lowery, M. D., and Solomon, E. I. (1995) Electronic structure of the reduced blue copper active site—contributions to reduction potentials and geometry, *J. Am. Chem. Soc. 117*, 2817−2844.
28. Hall, J. F., Kanbi, L. D., Strange, R. W., and Hasnain, S. S. (1999) Role of the axial ligand in type 1 Cu centers studied by point mutations of Met148 in rusticyanin, *Biochemistry 38*, 12675−12680.
29. Donaire, A., Jimenez, B., Moratal, J. M., Hall, J. F., and Hasnain, S. S. (2001) NMR studies on copper(II) rusticyanin: Is the Cu−SCys interaction responsible for the high redox potentials in blue copper proteins?, *Biochemistry 40*, 837−846.
30. Ryde, U., Olsson, M. H. M., Roos, B. O., De Kerpel, J. O. A., and Pierloot, K. (2000) On the role of strain in blue copper proteins, *J. Biol. Inorg. Chem. 5*, 565−574.
31. Berry, S. M., Ralle, M., Low, D. W., Blackburn, N. J., and Lu, Y. (2003) Probing the role of axial methionine in the blue copper center of azurin with unnatural amino acids, *J. Am. Chem. Soc. 125*, 8760−8768.
32. Murphy, M. E., Turley, S., Kukimoto, M., Nishiyama, M., Horinouchi, S., Sasaki, H., Tanokura, M., and Adman, E. T. (1995) Structure of *Alcaligenes feacalis* nitrite reductase and a copper site mutant, M150E, that contains zinc, *Biochemistry 34*, 12107−12117.
33. Olsson, M. H. M., Hong, G. Y., and Warshel, A. (2003) Frozen density functional free energy simulations of redox proteins: Computational studies of the reduction potential of plastocyanin and rusticyanin, *J. Am. Chem. Soc. 125*, 5025−5039.
34. Harrison, M. J., Burton, N. A., and Hillier, I. H. (1997) Catalytic mechanism of the enzyme papain: Predictions with a hybrid quantum mechanical molecular mechanical potential, *J. Am. Chem. Soc. 119*, 12285−12291.
35. Stephens, P. J., Jollie, D. R., and Warshel, A. (1996) Protein control of redox potentials of iron−sulfur proteins, *Chem. Rev. 96*, 2491−2513.
36. Field, M. J., Bash, P. A., and Karplus, M. (1990) A combined quantum chemical and molecular mechanical potential for molecular dynamics simulations, *J. Comput. Chem. 11*, 700−733.
37. Haladjian, J., Bruschi, M., Nunzi, F., and Bianco, P. (1993) Electron transfer reaction of rusticyanin, a blue copper protein from *Thiobacillus ferrooxidans*, at modified gold electrodes, *J. Electroanal. Chem. 352*, 329−335.
38. Murphy, L. M., Strange, R. W., Karlsson, B. G., Lundberg, L. G., Pascher, T., Reinhammar, B., and Hasnain, S. S. (1993) The structural characterization of azurin from *Pseudomonas aeruginosa* and some of its methionine-121 mutants, *Biochemistry 32*, 1965−1975.
39. Djebli, A., Proctor, P., Blake, R. C., and Shoham, M. (1992) Crystallisation and preliminary X-ray crystallographic studies of rusticyanin from *Thiobacillus ferrooxidans*, *J. Mol. Biol. 227*, 581−582.
40. Otwinowski, Z., and Minor, W. (1997) Processing of X-ray diffraction data collected in oscillation mode, in *Methods in Enzymology: Macromolecular Crystallography* (Carter, C. W., and Sweet, R. M., Eds.) Part A, pp 307−326, Academic Press, New York.
41. Potterton, E., Briggs, P., Turkenburg, M., and Dodson, E. (2003) A graphical user interface to the CCP4 program suite, *Acta Crystallogr., Sect. D 59*, 1131−1137.
42. Navaza, J. (1994) Amore—an automated package for molecular replacement, *Acta Crystallogr., Sect. A 50*, 157−163.
43. Brunger, A. T. (1992) X-PLOR Version 3.0 Manual.
44. Engh, R. A., and Huber, R. (1991) Accurate bond and angle parameters for X-ray protein structure refinement, *Acta Crystallogr., Sect. A 47*, 392−400.
45. Sheldrick, G. M., and Schneider, T. R. (1997) SHELXL: High-resolution refinement, in *Methods Enzymol. 277*, 319−343.
46. Jones, T. A., Zou, J. Y., Cowan, S. W., and Kjeldgaard, M. (1991) Improved methods for building protein models in electron density maps and the location of errors in these models, *Acta Crystallogr., Sect. A 47*, 110−119.
47. Laskowski, R. A., MacArthur, M. W., Moss, D. S., and Thornton, J. M. (1993). Procheck: a program to check the stereochemical quality of protein structures, *J. Appl. Crystallogr. 25*, 283−291.
48. Murshudov, G. N., Vagin, A. A., and Dodson, E. J. (1997) Refinement of macromolecular structures by the maximum-likelihood method, *Acta Crystallogr. 53*, 240−255.
49. Lamzin, V. S., and Wilson, K. S. (1993) Automated refinement of protein models, *Acta Crystallogr., Sect. D 49*, 129−147.
50. Kleywegt, G. J., and Jones, T. A. (1996) Efficient rebuilding of protein structures, *Acta Crystallogr., Sect. D 52*, 829−832.
51. Szilagyi, R. K., Metz, M., and Solomon, E. I. (2002) Spectroscopic calibration of modern density functional methods using $[CuCl_4]$-(2−), *J. Phys. Chem. A 106*, 2994−3007.
52. Maseras, F., and Morokuma, K. (1995) IMOMM—A new integrated ab initio plus molecular mechanics geometry optimisation scheme of equilibrium structures and transition states, *J. Comput. Chem. 16*, 1170−1179.
53. Vreven, T., Morokuma, K., Farkas, O., Schlegel, H. B., and Frisch, M. J. (2003) Geometry optimization with QM/MM, ONIOM, and other combined methods. I. Microiterations and constraints, *J. Comput. Chem. 24*, 760−769.
54. Frisch, M. J., Trucks, G. W., Schlegel, H. B., Scuseria, G. E., Robb, M. A., Cheeseman, J. R., Montgomery, Jr., J. A., Vreven, T., Kudin, K. N., Burant, J. C., Millam, J. M., Iyengar, S. S., Tomasi, J., Barone, V., Mennucci, B., Cossi, M., Scalmani, G., Rega, N., Petersson, G. A., Nakatsuji, H., Hada, M., Ehara, M., Toyota, K., Fukuda, R., Hasegawa, J., Ishida, M., Nakajima, T., Honda, Y., Kitao, O., Nakai, H., Klene, M., Li, X., Knox, J. E., Hratchian, H. P., Cross, J. B., Bakken, V., Adamo, C., Jaramillo, J., Gomperts, R., Stratmann, R. E., Yazyev, O., Austin, A. J., Cammi, R., Pomelli, C., Ochterski, J. W., Ayala, P. Y., Morokuma, K., Voth, G. A., Salvador, P., Dannenberg, J. J., Zakrzewski, V. G., Dapprich, S., Daniels, A. D., Strain, M. C., Farkas, O., Malick, D. K., Rabuck, A. D., Raghavachari, K., Foresman, J. B., Ortiz, J. V., Cui, Q., Baboul, A. G., Clifford, S., Cioslowski, J., Stefanov, B. B., Liu, G., Liashenko, A., Piskorz, P., Komaromi, I., Martin, R. L., Fox, D. J., Keith, T., Al-Laham, M. A., Peng, C. Y., Nanayakkara, A., Challacombe, M., Gill, P. M. W., Johnson, B., Chen, W., Wong, M. W., Gonzalez, C., and Pople, J. A. (2004) GAUSSIAN 03, Revision C.02, Gaussian, Inc., Wallingford, CT.
55. Case, D. A., Pearlman, D. A., Caldwell, J. W., Cheatham, T. E., III, Wang, J., Ross, W. S., Simmerling, C. L., Darden, T. A., Merz, K. M., Stanton, R. V., Cheng, A. L., Vincent, J. J., Crowley, M., Tsui, V., Gohlke, H., Radmer, R. J., Duan, Y., Pitera, J., Massova, I., Seibel, G. L., Singh, U. C., Weiner, P. K., and Kollmann, P. A. (2002) AMBER7.
56. Jorgensen, W. L., and Tiradorives, J. (1988) The OPLS potential functions for proteins—energy minimisations for cyclic peptides and crambin, *J. Am. Chem. Soc. 110*, 1657−1666.
57. Comba, P., and Remenyi, R. (2002) A new molecular mechanics force field for the oxidized form of blue copper proteins, *J. Comput. Chem. 23*, 697−705.
58. Merritt, E. A. (1999) Expanding the model: anisotropic displacement parameters in protein structure refinement, *Acta Crystallogr., Sect. D 55*, 1109−1117.
59. Cheung, K. C., Strange, R. W., and Hasnain, S. S. (2000) 3D EXAFS refinement of the Cu site of azurin sheds light on the nature of structural change at the metal centre in an oxidation−reduction process: an integrated approach combining EXAFS and crystallography, *Acta Crystallogr., Sect. D 56*, 697−704.
60. Hasnain, S. S., and Strange, R. W. (2003) Marriage of XAFS and crystallography for structure−function studies of metalloproteins, *J. Synchrotron Radiat. 10*, 9−15.
61. Strange, R. W., Eady, R. R., Lawson, D., and Hasnain, S. S. (2003) XAFS studies of nitrogenase: the MoFe and VFe proteins and the use of crystallographic coordinates in three-dimensional EXAFS data analysis, *J. Synchrotron Radiat. 10*, 71−75.
62. Strange, R. W., Reinhammar, B., Murphy, L. M., and Hasnain, S. S. (1995) Structural and spectroscopic studies of the copper site of stellacyanin, *Biochemistry 34*, 220−231.

63. Xiao, Z., Gardner, A. R., Cross, M., Maes, E. M., Czernuszewicz, R. S., Sola, M., and Wedd, A. G. (2001) Redox thermodynamics of mutant forms of the rubredoxin from *Clostridium pasteurianum*: identification of a stable Fe-111 (S-Cys)(3)(OH) centre in the C6S mutant, *J. Biol. Inorg. Chem. 6*, 638−649.
64. Xiao, Z. G., Lavery, M. J., Ayhen, M., Scrofani, S. D. B., Wilce, M. C. J., Guss, J. M., Tregloan, P. A., George, G. N., and Wedd, A. G. (1998) The rubredoxin from *Clostridium pasteurianum*: Mutation of the iron cysteinyl ligands to serine. Crystal and molecular structures of oxidized and dithionite-treated forms of the Cys42Ser mutant, *J. Am. Chem. Soc. 120*, 4135−4150.
65. Sundararajan, M., Hillier, I. H., and Burton, N. A. (2006) Structure and redox properties of the protein, rubredoxin, and its ligand and metal mutants studied by electronic structure calculation, *J. Phys. Chem. A 110*, 785−790.

BI052372W